Accessibility of the surface fractal dimension during film growth

Edwin E. Mozo Luis,[1,*] Fernando A. Oliveira [1,2,3,†] and Thiago A. de Assis [1,3,‡]

[1]*Instituto de Física, Universidade Federal da Bahia, Campus Universitário da Federação,*
Rua Barão de Jeremoabo s/n, 40170-115, Salvador, BA, Brazil
[2]*Instituto de Física, Universidade de Brasília, 70910-900, Brasília, DF, Brazil*
[3]*Instituto de Física, Universidade Federal Fluminense, Avenida Litorânea s/n, 24210-340, Niterói, RJ, Brazil*

Fractal properties on self-affine surfaces of films growing under nonequilibrium conditions are important in understanding the corresponding universality class. However, measurement of the surface fractal dimension has been intensively investigated and is still very problematic. In this work, we report the behavior of the effective fractal dimension in the context of film growth involving lattice models believed to belong to the Kardar-Parisi-Zhang (KPZ) universality class. Our results, which are presented for growth in a d-dimensional substrate ($d = 1, 2$) and use the three-point sinuosity (TPS) method, show universal scaling of the measure M, which is defined in terms of discretization of the Laplacian operator applied to the height of the film surface, $M = t^\delta g[\Theta]$, where t is the time, $g[\Theta]$ is a scale function, $\delta = 2\beta$, $\Theta \equiv \tau t^{-1/z}$, β, and z are the KPZ growth and dynamical exponents, respectively, and τ is a spatial scale length used to compute M. Importantly, we show that the effective fractal dimensions are consistent with the expected KPZ dimensions for $d = 1, 2$, if $\Theta \lesssim 0.3$, which include a thin film regime for the extraction of the fractal dimension. This establishes the scale limits in which the TPS method can be used to accurately extract effective fractal dimensions that are consistent with those expected for the corresponding universality class. As a consequence, for the steady state, which is inaccessible to experimentalists studying film growth, the TPS method provided effective fractal dimension consistent with the KPZ ones for almost all possible τ, i.e., $1 \lesssim \tau < L/2$, where L is the lateral size of the substrate on which the deposit is grown. In the growth of thin films, the true fractal dimension can be observed in a narrow range of τ, the upper limit of which is of the same order of magnitude as the correlation length of the surface, indicating the limits of self-affinity of a surface in an experimentally accessible regime. This upper limit was comparatively lower for the Higuchi method or the height-difference correlation function. Scaling corrections for the measure M and the height-difference correlation function are studied analytically and compared for the Edwards-Wilkinson class at $d = 1$, yielding similar accuracy for both methods. Importantly, we extend our discussion to a model representing diffusion-dominated growth of films and find that the TPS method achieves the corresponding fractal dimension only at steady state and in a narrow range of the scale length, compared to that found for the KPZ class.

I. INTRODUCTION

Scale invariance and fractality are expected to emerge for growth far from equilibrium [1]. In the context of film growth [2,3], determining the scaling properties of the roughness during the kinetic roughening stage has been a source of intense research [1,3–13].

The squared roughness is defined by

$$w^2(L,t) \equiv \langle \overline{h^2(\mathbf{x},t)} - \overline{h(\mathbf{x},t)}^2 \rangle, \tag{1}$$

where $h(\mathbf{x}, t)$ is the interface height, which evolves on time t perpendicularly to a d-dimensional substrate. L is the lateral size of the substrate, and overbars and brackets indicate the spatial and configurational averages, respectively. For many growth processes, including film growth, $w(L, t)$ increases with time via a power law, which is an experimentally accessible regime. However, at sufficiently long times, $w(L, t)$ is expected to reach a steady state with saturated roughness w_s, i.e., $w(L, t \to \infty) = w_s$. Then, the surface global roughness evolves over time as:

$$w(L,t) = \begin{cases} ct^\beta, & \text{if } t \ll t_\times \\ w_s \sim L^\alpha, & \text{if } t \gg t_\times \end{cases} \tag{2}$$

with $t_\times \sim L^z$. In a normal scaling regime, in which the Family-Vicsek [3,14,15] ansatz holds, $z = \alpha/\beta$, the scaling exponents α, β and z, i.e., the roughness, growth, and dynamic exponents, respectively, define the universality class of the growth process.

Indeed, the possibility of characterizing the morphology of an irregular surface experimentally at the nanometer up to µm scales requires, for example, scanning probe microscopy [16]. This has stimulated an upsurge in experimental reports claiming self-affine structures. Of course, care is necessary, since the finite size of the probe tip does not enable full

*mozo2920@gmail.com
†faooliveira@gmail.com
‡thiagoaa@ufba.br

resolution of neither deep valleys nor sloping borders of plateaus on the interfaces analyzed [16–18].

Prior work has involved experimental studies of the morphology of thin solid films and estimated their surface fractal dimension [19]. For example, Zhu *et al.* studied evolution of the film morphologies of organic semiconductors [20] and measured the fractal dimensions during thin film growth (i.e., $t \ll t_x$). Kavyashree *et al.* [21] measured fractal dimension to explore how different substrates affect the morphologies of deposited barium fluoride (BaF$_2$) thin films. Țălu *et al.* [22] studied Ag/Cu thin films deposited on (001)-oriented Si via reactive dc magnetron sputtering and investigated the self-affine nature of the sample morphology. Ghosh *et al.* calculated the fractal dimension of surface microstructures for sol-gel spin coated ZnO thin films with varying precursor molarities [23]. A recent study revisited fractal analyses of thin film surfaces and reinforced the importance of the fractal dimension in exploring the mechanisms of film growth under different conditions [24].

However, it is important to understand under which conditions the fractal dimension is a reliable quantity to determine the underlying dynamics of surface growth and, consequently, help to understand and improve materials production. In this work, we investigate this problem in the context of lattice models of film growth, for a class of kinetic roughening processes characterized by nonconserved surface relaxation.

This problem has been stimulated, at a coarse-grained level [11], for the Kardar-Parisi-Zhang (KPZ) class, for which the space-time evolution of $h(\mathbf{x}, t)$ is given by the KPZ Eq. [5],

$$\frac{\partial h(\mathbf{x}, t)}{\partial t} = \nu \nabla^2 h(\mathbf{x}, t) + \frac{\lambda}{2}[\nabla h(\mathbf{x}, t)]^2 + \eta(\mathbf{x}, t). \quad (3)$$

The parameters ν, i.e., surface tension, and λ are related to Laplacian smoothing and the tilt mechanism, respectively. The scaling properties of $h(\mathbf{x}, t)$ are different from those of $\mathbf{x}$. Therefore, we refer to this situation as a $d + 1$ growth. The stochastic process is characterized by the noise, $\eta(\mathbf{x}, t)$, which in its simplest form is white noise:

$$\langle \eta(\mathbf{x}, t)\eta(\mathbf{x}', t') \rangle = 2D\delta^d(\mathbf{x} - \mathbf{x}')\delta(t - t'), \quad (4)$$

where D is the noise intensity.

For a film growing in $2 + 1$ dimensions, one possible way to determine the corresponding global roughness exponent is to measure $h(\mathbf{x}, t)$ along a single line in the x plane [25]. In this work, this section through the surface is analyzed as if it were a one-dimensional profile, and averages are taken over many profiles along directions x and y parallel to the substrate to calculate the effective fractal dimensions. This suggests a relationship between the global roughness exponent and the fractal dimension of the profile in a steady state, which is experimentally inaccessible for studies of film growth. In such cases it is possible to write [3]:

$$\alpha = 2 - d_f, \quad d = 1, 2. \quad (5)$$

Therefore, regarding one of the challenges described previously, a relevant issue is: is the surface fractal dimension extracted, for the growth regime ($t \ll t_x$), connected with the corresponding universality class?

II. LATTICE MODELS AND METHOD

In order to investigate this issue, we consider three well-known KPZ lattice models, namely: the etching [9], restricted solid-on-solid (RSOS) [26], and single step (SS) models [25,27–29]. We explore the situations for $d = 1, 2$, which encompasses cases with experimental relevance. For the presentation of simulation results along this work, we consider the lattice constant as the unit length, i.e., $a = 1$. In general, at time t, we randomly choose a column of the deposit in R^d space. Time unity corresponds to a deposition of L^d particles. All simulations have been performed by considering periodic boundary conditions and an initial substrate with $h(\mathbf{x}, 0) = 0$, except with the SS model, for which $h_i = [1 + (-1)^i]/2$ for $d = 1$ and $h_{i,j} = [1 + (-1)^{i+j}]/2$ for $d = 2$ [$1 \leqslant (i, j) \leqslant L$]. The etching model is an automaton that mimics erosion of a surface with acid [9,30–35], and it was recently [36] proved to belong to the KPZ universality class. Here, this model was simulated in its deposition version in order to be consistent with film growth. After each deposition attempt, the height of the column of incidence, h_0, was increased by one lattice unit and any neighboring column with a height smaller than h_0 increased until its height was h_0. In the RSOS model, an incident particle may stick at the top of the column of incidence if the difference in height between the incidence column and each of the neighboring columns does not exceed one lattice unit. Otherwise, deposition is rejected. The SS model [25,27–29] (for a more recent work, see Ref. [37]) is defined as follows: at any time t, if the column height of a randomly selected site is a local minimum, then it is increased by two lattice parameters with probability p. Otherwise, if we have a maximum, the column height is decreased by two lattice parameters with probability $1 - p$. In this work we present the results for the SS model considering $p = 1$.

Next, we describe the method used in this work for calculation of the fractal dimension. The method used here was the three-point sinuosity (TPS) method, which was introduced in Ref. [38]. This method can be described as follows: at a given time t, a discrete irregular interface with height h_i, where $i = 1, \ldots, L$, is considered. Given a height h_i, two heights $h_{i+\tau}$ and $h_{i+2\tau}$ are determined, with $1 \leqslant \tau < L/2$ being the horizontal scale length. The local TPS, ρ_i^τ, with i and τ fixed is defined by [38]

$$\rho_i^\tau = |2h_{i+\tau} - h_i - h_{i+2\tau}|. \quad (6)$$

Equation (6) is related to discretization of the Laplacian operator in one dimension. Therefore, ρ_i^τ represents the sinuosity of the curve formed by heights h_i, $h_{i+\tau}$, and $h_{i+2\tau}$ in the range $[i, i + 2\tau]$. In this range, a peak, a valley, and a downward or a upward slope can be observed. For the whole interface, a series of ρ_i^τ was achieved and a measure M was defined as:

$$M = \frac{1}{L - 2\tau} \sum_{i=1}^{L-2\tau} (\rho_i^\tau)^2. \quad (7)$$

The measure M scales with τ as [38]

$$M \sim \tau^{4 - 2d_f^{\mathrm{TPS}}}, \quad (8)$$

where d_f^{TPS} is the surface fractal dimension extracted with the TPS method. With this method, a fractal dimension with an
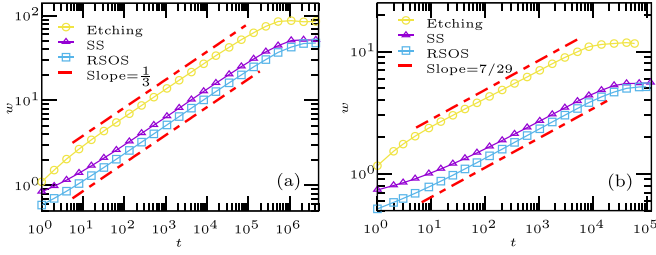
FIG. 1. Global roughness, $w(L, t)$, as a function of time, t, considering the etching, SS and RSOS models. (a) Results for $d = 1$ with lateral size $L = 2^{15}$ for an average over 10^3 independent realizations. Dashed (red) lines indicate slopes equal to $1/3$. (b) Results for $d = 2$ considering the lateral sizes $L = 2^{11}$ for etching model and $L = 2^{10}$ for the SS and RSOS models. Dashed (red) lines indicate slopes equal to $7/29$ (e.g., see Ref. [43]).

irregular discrete surface can be numerically evaluated at each time t. Indeed, under conditions in which a power-law dependence between M and τ is observed, i.e., the profile is scale invariant, the exponent $C \equiv 4 - 2d_f^{\text{TPS}}$ can be determined by using a least-squares procedure [39] and $d_f^{\text{TPS}} = 2 - C/2$ [38]. In this work, instead, an effective fractal dimension, $d_{f_{\text{eff}}}^{\text{TPS}}$, was computed and defined as in Eq. (8):

$$d_{f_{\text{eff}}}^{\text{TPS}} \equiv 2 - \frac{1}{2} \frac{d[\ln (M)]}{d[\ln (\tau)]}. \tag{9}$$

III. RESULTS AND DISCUSSION

Figure 1(a) shows the time evolution of the global roughness, $w(L, t)$, for $L = 2^{15}$, as determined by considering the etching, RSOS and SS models for $d = 1$. The results are presented as averages over 10^3 independent realizations. Figure 1(b) shows the time evolution of $w(L, t)$ for the same models in Fig. 1(a), but with $d = 2$. In this case $L = 2^{11}$ for the etching model whereas $L = 2^{10}$ for the RSOS and SS models. The results for $d = 2$ are shown by considering an average over 10^3 independent realizations for the SS and RSOS models. For the etching model, the results are presented for 400 independent realizations. Clearly, for short times after an initial transient, $w(t) \sim t^\beta$ for all models, with $\beta \approx 1/3$ for $d = 1$ and, for $d = 2$, β was close to those reported in the literature for the KPZ models (e.g., see Refs. [11,40–43] and $\beta = 7/29$ in Ref. [43]).

A characteristic surface length can be extracted for the simulated interfaces from the autocorrelation function, which is defined as

$$\Gamma(\mathbf{r}, t) = \langle \tilde{h}(\mathbf{r_0} + \mathbf{r}, t) \tilde{h}(\mathbf{r}, t) \rangle, \tag{10}$$

where $\tilde{h} = h - \bar{h}$, $\bar{h}$ is the mean height of the profile, and averages in Eq. (10) were performed over different reference positions $\mathbf{r_0}$, different orientations, and independent samples.

The correlation length, ξ, is often estimated as the position of the first zero or minimum of $\Gamma(\mathbf{r}, t)$ [32,44]. However, in such cases, $\Gamma(\mathbf{r}, t)$ may oscillate with r before crossing the value $\Gamma = 0$ [45,46]. For this reason, we define ξ here as $\Gamma(\xi, t)/\Gamma(\mathbf{0}) = 0.3$ [45], where $\Gamma(\mathbf{0}) \equiv \Gamma(\mathbf{0}, t)$. The reliability of this approach has been demonstrated for KPZ lattice models [45] and confirmed for the models studied here. In the
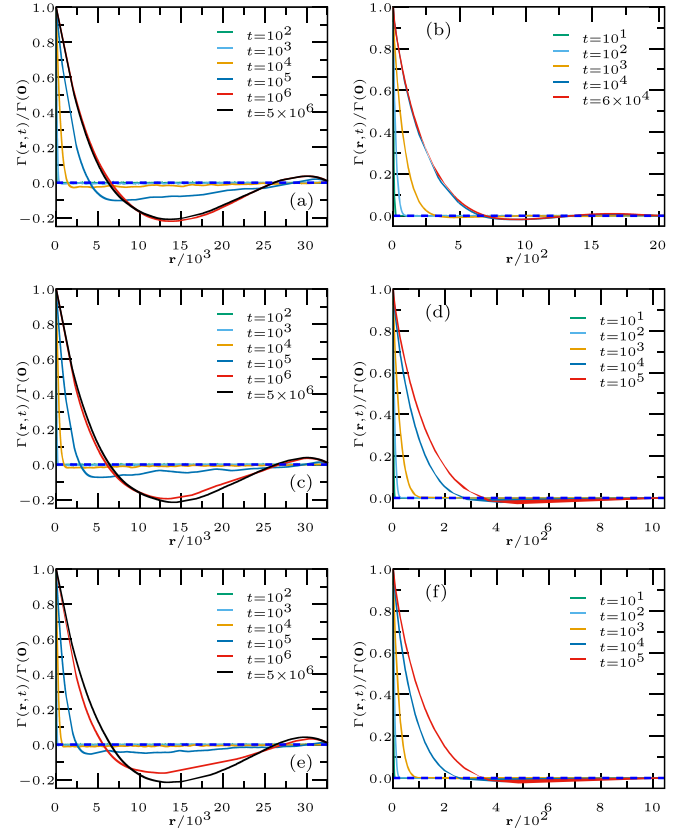

FIG. 2. $\Gamma(\mathbf{r}, t)/\Gamma(\mathbf{0})$ as a function of r, for different times, for (left panels) $d = 1$ and (right panels) $d = 2$. (a) and (b), (c) and (d), and (e) and (f) correspond to the results for the SS, etching, and RSOS models, respectively.

growth regime ($t \ll t_x$), ξ scales as $\xi(t) \sim t^n$, where $n \equiv 1/z$ is the coarsening exponent, which is usually the inverse of the dynamic exponent, as defined previously. The calculated (normalized) correlation functions $\Gamma(\mathbf{r}, t)/\Gamma(\mathbf{0})$ are shown in Fig. 2. The time evolution of ξ and its values are shown in Fig. 3 and Table I, respectively. Our results show that ξ scales approximately as $\xi \sim t^{1/z}$ for $t \lesssim 10^4$ and $d = 1, 2$, which
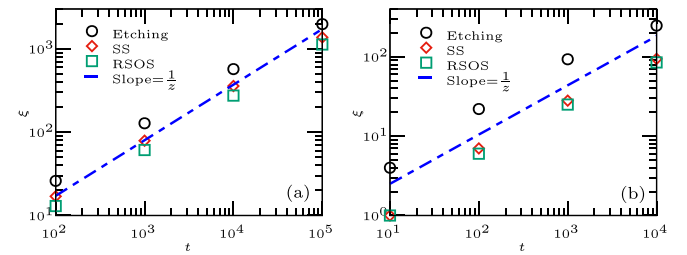

FIG. 3. Evolution of the correlation length, ξ (see Table I) for the etching, SS and RSOS models. (a) Results for $d = 1$ are shown for the lateral size $L = 2^{15}$ and were averaged over 10^3 independent experiments. The dashed (blue) line shows a slope equal to $1/z$ with $z = 3/2$. (b) Results for $d = 2$ using the lateral sizes $L = 2^{11}$ for the etching model (4×10^2 independent experiments) and $L = 2^{10}$ for the SS and RSOS models, averaged over 10^3 independent experiments. The dashed (blue) line indicates a slope equal to $1/z$, where $z = 29/18$ (e.g., see Ref. [43]).

TABLE I. Values of ξ, for different values of t, for the models SS, etching and RSOS. Results are shown for $d = 1, 2$ and were obtained from Fig. 2 considering $\Gamma(\xi, t)/\Gamma(\mathbf{0}) = 0.3$ [45].

d	t	ξ^{Etching}	ξ^{SS}	ξ^{RSOS}
	10^2	26	17	13
	10^3	128	79	61
1	10^4	571	358	274
	10^5	1975	1369	1126
	10^6	3500	3170	2918
	5×10^6	3388	3467	3599
	10^1	4	1	1
	10^2	22	7	6
2	10^3	93	28	25
	10^4	247	94	85

is consistent with the results in Ref. [45]. For sufficiently large times (i.e., $t \gtrsim 10^4$, where finite-size effects become important, see Fig. 1), the effective ξ grows more slowly than $t^{1/z}$, as we will show next (see the arrows in the left and right panels of Figs. 4 and 5). Figures 4(a), 4(c) and 4(e) show the measured M, which was computed by using Eq. (7), as a function of the spatial horizontal scale length, τ, for the etching, SS, and RSOS models in $d = 1$, respectively. Various times t, encompassing the growth and the steady-state region were considered, as observed in Fig. 1. These results showed that, for $1 \lesssim \tau \lesssim \xi$, M scales as in Eq. (8). Furthermore, for $t \ll t_x$, the scale invariance of the irregular profiles does not extend to all length scales exhibiting an upper limit length, $\ell \sim \xi$. For $\tau \gtrsim \xi$, scale invariance of the profile was no longer observed and M was converted to a constant value. For times corresponding to the steady state, $t \gg t_x$, Eq. (8) holds for the whole range of τ.

The insets of Figs. 4(a), 4(c) and 4(e) show the excellent collapse achieved by replacing the variables $M \rightarrow Mt^{-\delta}$ and $\tau \rightarrow \Theta \equiv \tau t^{-1/z}$, where, for $d = 1$, $\delta = 2\beta = 1/z$, and $z = 1.5$, the latter corresponds to the KPZ dynamic exponent for $d = 1$. Therefore, we propose scaling as $M = t^\delta g[\Theta]$, where $\Theta \equiv \tau t^{-1/z}$. Using Eq. (8), the function $g[\Theta]$ is expected to scale as:

$$g[\Theta] \sim \begin{cases} \Theta^{4-2d_f^{\text{TPS}}}, & \text{if } \Theta \ll 1; \\ cte, & \text{if } \Theta \gg 1. \end{cases} \quad (11)$$

Indeed, for $\Theta \ll 1$, $4 - 2d_f^{\text{TPS}}$ is expected to be exactly unity. This was confirmed by the slopes shown in the insets of Figs. 4(a), 4(c) and 4(e), where the dashed lines have slopes equal to unity. Of course, for $\Theta \gg 1$, $M \sim t^{1/z}$.

Figures 4(b), 4(d) and 4(f) show the effective fractal dimensions computed using Eq. (9) as a function of $\Theta \equiv \tau t^{-1/z}$, for the etching, SS and RSOS models in $d = 1$, respectively. The results are presented for the same times represented in the left panels. Importantly, good collapse of the curves for all models studied here indicated that an effective fractal dimension consistent with that for KPZ could be achieved for $\Theta = \tau t^{-1/z} \lesssim 0.3$. This result established the limits of τ to be used in the TPS method for a given time t in order to observe an effective fractal dimension consistent with the KPZ class. It is interesting to note that, for the steady state,
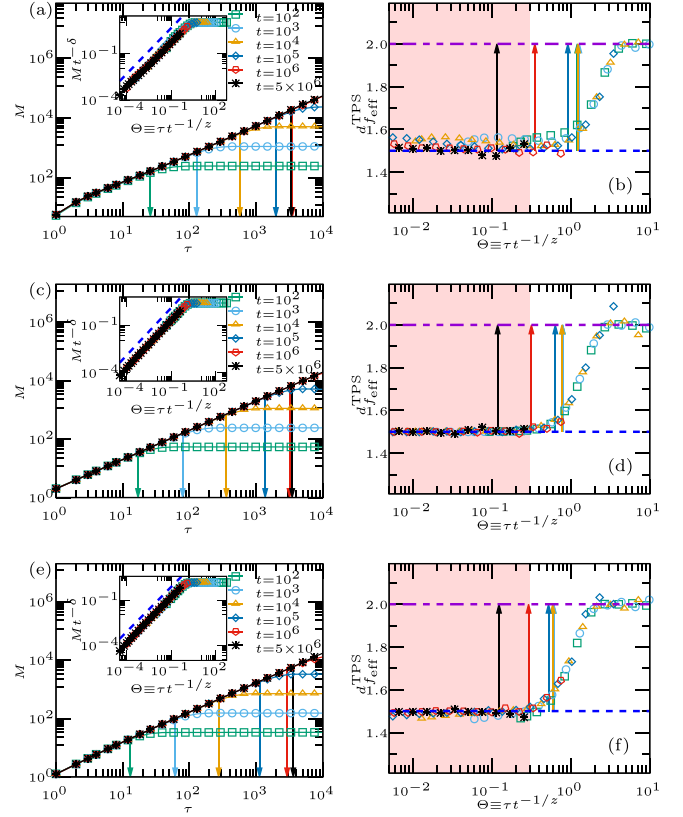

FIG. 4. Results for $d = 1$. (Left panels) M as a function of τ. Vertical arrows indicate, for each time, the position $\tau = \xi$ (see Table I). (Right panels) $d_{f_{\text{eff}}}^{\text{TPS}}$ as a function of $\Theta \equiv \tau t^{-1/z}$. Vertical arrows indicate, for each time, the position at $\Theta = \xi t^{-1/z}$. We note that $\xi t^{-1/z}$ is nearly constant for $t \lesssim 10^4$ (the arrows overlap at these times). (a) and (b) for etching model; (c) and (d) for the SS model; (e) and (f) for the RSOS model. The results are presented for lateral size $L = 2^{15}$, with averages calculated for 10^3 independent realizations. In (a), (c), and (e), the insets show collapse achieved by replacing the variables $M \rightarrow Mt^{-\delta}$ and $\tau \rightarrow \Theta \equiv \tau t^{-1/z}$, where, for $d = 1$, $\delta = 2\beta = 1/z$, with $z = 1.5$. Dashed lines have slope 1. In (b), (d), and (f), the results are presented for $\tau \geqslant 3$ and dashed horizontal bottom and top lines represent the values of the KPZ fractal dimension, for $d = 1$, using Eq. (5) $[d_f = 2 - \alpha = 1.5]$, and the value 2, respectively. The pink area shows a limit for the variable $\Theta \equiv \tau t^{-1/z}$, where the KPZ fractal dimension could be achieved.

all values $1 \lesssim \tau < L/2$ could be used to provide the correct fractal dimension. However, the steady-state regime is not experimentally accessible in the context of film growth.

Indeed, in the limit of thin film growth, i.e., $t \ll t_x$, $d_{f_{\text{eff}}}^{\text{TPS}}$ crosses over and subsequently converges to 2 for almost all values of τ, since M rapidly reaches a constant value. This suggested that an effective fractal dimension close to 2, as determined with the TPS technique, represented an uncorrelated profile inconsistent with that expected for the KPZ universality class in $d = 1$ (i.e., $d_f = 1.5$). Therefore, within the limit of thin film growth, a narrow range of τ, consistent with $\Theta = \tau t^{-1/z} \lesssim 0.3$, should allow one to obtain the KPZ fractal dimension.

The results discussed above were also confirmed for the case $d = 2$, where realistic applications can be found.
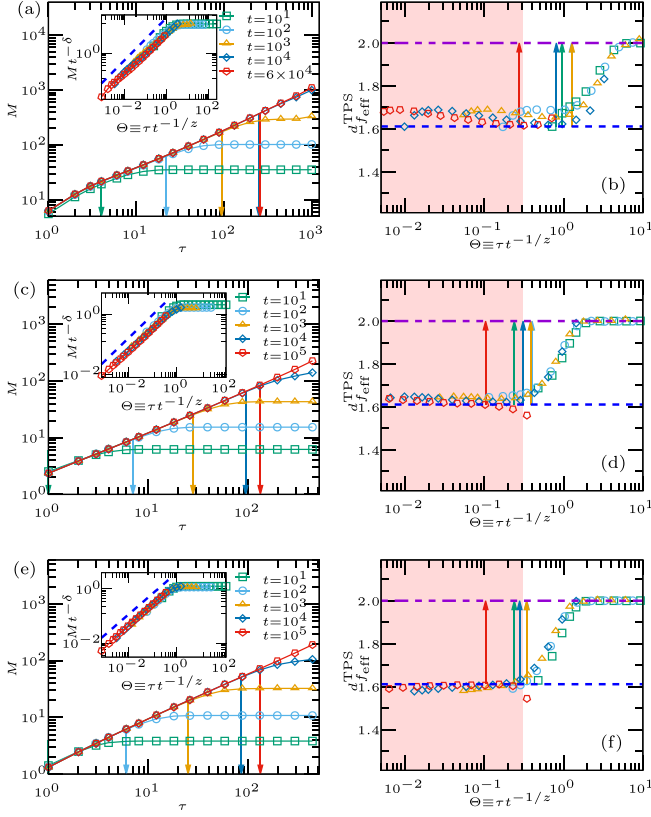
FIG. 5. Results for $d = 2$. (Left panels) M as a function of τ. Vertical arrows indicate, for each time, the position $\tau = \xi$ (see Table I). (Right panels) $d_{f_{\text{eff}}}^{\text{TPS}}$ as a function of $\Theta \equiv \tau t^{-1/z}$. Vertical arrows indicate, for each time, the position at $\Theta = \xi t^{-1/z}$. We note that $\xi t^{-1/z}$ is nearly constant for $t \lesssim 10^4$ (striking is the overlapping of the arrows at times $10^2 \lesssim t \lesssim 10^3$). (a) and (b) for the etching model; (c) and (d) for the SS model; (e) and (f) for the RSOS model. The results are presented for lateral sizes $L = 2^{11}$ for etching with 400 independent realizations and $L = 2^{10}$ for the SS and RSOS models with 10^3 independent realizations. In (a), (c), and (e), the insets show the collapse achieved by replacing the variables $M \to Mt^{-\delta}$ and $\tau \to \tau t^{-1/z}$, where $z = 29/18$ (e.g., Ref. [43]). In (a), (c), and (e), the dashed lines have slopes $2\alpha = 7/9$ and the values of the exponent δ used were $\delta = 2\beta = 14/29$ [43]. In (b), (d), and (f), the results are presented for $\tau \geqslant 3$ and the dashed horizontal top and bottom lines represent the value of the KPZ fractal dimension, that, for $d = 2$, using Eq. (5), is $d_f = 29/18$ (using α reported in Ref. [43]), and the value 2, respectively. The pink area shows an approximate limit for the variable $\Theta \equiv \tau t^{-1/z}$, from which the KPZ fractal dimension could be achieved.

Accordingly, Figs. 5(a), 5(c) and 5(e) show the measured M as a function of τ for the etching, SS, and RSOS models, respectively. These results confirmed again that M scales as in Eq. (8) for $\tau \lesssim \xi$. For $\tau \gtrsim \xi$, M is constant, similar to the result found for $d = 1$.

The insets of the Figs. 5(a), 5(c) and 5(e) show excellent collapse achieved by replacing the variables $M \to Mt^{-\delta}$ and $\tau \to \tau t^{-1/z}$, for which we used $z = 29/18$ as the KPZ dynamic exponent, as reported in Ref. [43], for $d = 2$. Therefore, the scaling model $M = t^{\delta} g[\Theta]$ is proposed, where $\delta = 2\beta = 14/29$ (for $d = 2$) [43] and $\Theta \equiv \tau t^{-1/z}$, as previously defined.

Figures 5(b), 5(d) and 5(f) show the effective fractal dimensions as a function of $\Theta \equiv \tau t^{-1/z}$ for the etching, SS, and RSOS models with $d = 2$, respectively. The same trends were observed, so that, for $t \ll t_x$, $d_{f_{\text{eff}}}^{\text{TPS}}$ rapidly converged to 2, when M converged rapidly to a constant value. The effective fractal dimensions are consistent with those expected for the KPZ model at steady state, where a clear plateau is observed for $1 \lesssim \tau < L/2$. (For $d = 2$, two recent works found $d_f = (1 + \sqrt{5})/2 \approx 1.618$, see Ref. [11], or $d_f = 29/18$, see Ref. [43]. Note that our numerical results are not accurate enough to distinguish between these fractal dimensions.) Furthermore, the good collapse of the curves, similar to that achieved for $d = 1$, indicated that an effective fractal dimension consistent with that for KPZ could be achieved, even in a thin film growth, for $\Theta = \tau t^{-1/z} \lesssim 0.3$. We emphasise that the good collapses from Fig. 5 were also observed when the KPZ exponents reported in Ref. [42] are considered [i.e., $\alpha = 0.390(4)$ and $\beta = 0.241(1)$]. Of course, the KPZ scaling exponents in $d > 1$ are a source of intense research (e.g., Refs. [11,42,43,47]).

IV. RESULTS FOR HIGUCHI METHOD

The agreement of the effective fractal dimensions defined by Eq. (9) with those of the KPZ class for $d = 1, 2$ observed by the TPS method was also observed by the well-known Higuchi method [48,49], but in a more limited range of scale lengths, even at steady state.

To show these results, we first present the Higuchi method (HM) [48,49] and our results for computing the effective fractal dimension. In the following, the effective fractal dimension numerically calculated by this method will be referred to as $d_{f_{\text{eff}}}^{\text{HM}}$. The method HM can be described as follows: for a given discrete boundary surface with height h_i associated with the ith site and lateral dimension L, one can construct a new interface represented by h_m^k, where m and k are integers representing the denotation of an initial site and the interval in which a new height is reached, respectively. It is possible to define the floor function of $(L - m)/k$, $\mathcal{M} \equiv \lfloor (L - m)/k \rfloor$. For each new profile with height $\{h_m^k\}$, an average length $\mathcal{L}_m^k$ can be defined as:

$$\mathcal{L}_m^k \equiv \frac{1}{k}\left\{ \frac{L-1}{\mathcal{M}k} \sum_{i=1}^{\mathcal{M}} (|h_{m+ik} - h_{m+(i-1)k}|) \right\}. \quad (12)$$

The term $(L - 1)/\mathcal{M}k$ corresponds to the normalization factor for the curve lengths of the subprofiles. The length $\mathcal{L}_k$ of the curve for each interval k is then estimated as:

$$\mathcal{L}_k = \frac{1}{k} \sum_{m=1}^{k} \mathcal{L}_m^k. \quad (13)$$

Since $\mathcal{L}_k$ scales as $(k)^{-d_f^{\text{HM}}}$, then:

$$\log_{10}(\mathcal{L}_k) \sim -d_f^{\text{HM}} \log_{10}(k). \quad (14)$$

The prefactor $-d_f^{\text{HM}}$ can be calculated numerically using a least-squares method [39]. As with the TPS method, we can also define an effective fractal dimension $d_{f_{\text{eff}}}^{\text{HM}}$. In this section, we present the results only for the RSOS model in $d = 1, 2$.
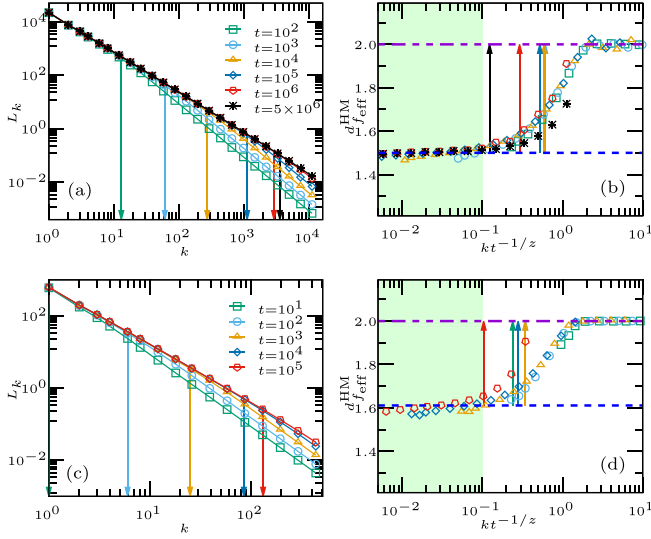
FIG. 6. Results for $d = 1$ in (a) and (b) [$d = 2$ in (c) and (d)]. (Left panels) L_k as a function of k. Vertical arrows indicate, for each time, the position $\tau = \xi$ (see Table I). (Right panels) $d_{f_{\text{eff}}}^{\text{HM}}$ as a function of $kt^{-1/z}$. Vertical arrows indicate, for each time, the position at $\xi t^{-1/z}$. The results are presented for the RSOS model with lateral size $L = 2^{15}$ ($L = 2^{10}$) for $d = 1$ ($d = 2$), with averages calculated for 10^3 independent realizations. In (b) and (d), dashed horizontal bottom and top lines represent the values of the KPZ fractal dimension for $d = 1, 2$, using Eq. (5) [$d_f = 2 - \alpha$], and the value 2, respectively. The green area shows a limit for the variable $kt^{-1/z}$, where the KPZ fractal dimension could be achieved.

The results for the other KPZ models studied here lead to similar conclusions, as explained below.

Figures 6(a) and 6(c) show $\mathcal{L}_k$ as a function of k, considering the RSOS model, for $d = 1$ and $d = 2$, respectively, for different times. For $d = 1$ and $d = 2$, the results are presented for lateral sizes $L = 2^{15}$ and $L = 2^{10}$, respectively. In both cases, 10^3 independent experiments were considered. Vertical arrows indicate, for each time, the position $k = \xi$.

Figures 6(c) and 6(d) show $d_{f_{\text{eff}}}^{\text{HM}}$ as a function of $kt^{-1/z}$. Vertical arrows indicate, for each time, the position $\xi t^{-1/z}$.

These results show that the scale interval in which the Higuchi method achieves a nearly KPZ effective fractal dimension is narrower (i.e., $kt^{-1/z} \lesssim 0.1$) than that of the TPS method. This indicates an advantage of the scaling interval of the TPS method over that of the Higuchi method. As for the accuracy, our numerical results for the range of scale lengths where the effective fractal dimensions are close to the KPZ class show no significant difference between the two methods. Therefore, it would be more appropriate to investigate this issue for situations where analytical calculations are possible. In this way, a more detailed discussion of accuracy due to scaling corrections for the TPS method is presented below.

V. ANALYSIS FOR OTHER UNIVERSALITY CLASSES

A. Edwards-Wilkinson (EW) class

1. Scaling corrections for the measure M

The EW equation [4] corresponds to the linear counterpart of the KPZ equation [$\lambda = 0$ in Eq. (3)]. This model belongs

to a class of Gaussian interface models in which the variance of the Fourier amplitudes is an exact power law of the wave number [50–52]. One could analytically derive the scaling corrections of the measure M and compare its accuracy with other measures commonly used to extract roughness exponents. In this discussion, we restrict our analysis to $d = 1$.

For this purpose, we assume that the discretization has a negligible effect for length scales of the same order of magnitude of the lattice parameter a, i.e., for $L \gg a$, as considered in this work. The squared global roughness defined in Eq. (1) can be written as [52]:

$$w^2(L, t) = \frac{AL}{\pi} \int_{2\pi/L}^{2\pi/a} \frac{dq}{Lq^\gamma}, \tag{15}$$

where $q \equiv 2\pi(n/L)$, A is a constant, $\gamma = 2$ for EW equation, and $n = \pm 1, \ldots, \pm L/a$.

For $r_0 = ma$ (m is an integer) [r_0 was previously given in Eq. (10)] as considered in lattice models, and neglecting a correction of order $(a/L)^{\gamma-1}$, the difference $\Delta \equiv \Gamma(r, t) - w^2(L, t)$ can be written [neglecting terms containing $(a/r)^p$ ($p \geqslant 3$)] as [52]:

$$\Delta \approx A\left[-c_1 r^{2\alpha} + c_2 a^{2\alpha} + c_3 a^{2\alpha}\left(\frac{a}{r}\right)^2\right], \tag{16}$$

where the coefficients c_p ($p = 1, 2, 3$) are constants.

On the other hand, from Eqs. (6) and (7), one readily obtains, for a given time t,

$$M = 6\Gamma(0) - 8\Gamma(r) + 2\Gamma(2r). \tag{17}$$

Of course, $\Gamma(0) = w^2$. Using Eqs. (16) and (17), one gets

$$M \approx K_M^I r^{2\alpha} + K_M^{II} + K_M^{III}\left(\frac{a}{r}\right)^2, \tag{18}$$

where $K_M^I = Ac_1[8 - 2^{(2\alpha+1)}]$, $K_M^{II} = -6Ac_2 a^{2\alpha}$, and $K_M^{III} = -(15/2)Ac_3 a^{2\alpha}$. Therefore, Eq. (18) shows the scaling corrections for the measure M.

To make a comparison with the corrections to other quantities, we obtain the ratios for the measure M as defined below:

$$R_{I,II,M} \equiv \frac{K_M^I}{K_M^{II}} = -\frac{c_1[8 - 2^{(2\alpha+1)}]}{6c_2}a^{-2\alpha}; \tag{19}$$

$$R_{I,III,M} \equiv \frac{K_M^I}{K_M^{III}} = -\frac{2c_1[8 - 2^{(2\alpha+1)}]}{15c_3}a^{-2\alpha}; \tag{20}$$

and

$$R_{II,III,M} \equiv \frac{K_M^{II}}{K_M^{III}} = \frac{4c_2}{5c_3}. \tag{21}$$

2. Comparison with height difference correlation function

The height difference correlation function is defined as [52,54]:

$$G(r, t) \equiv \overline{\langle [h(\mathbf{r_0} + \mathbf{r}, t) - h(\mathbf{r}, t)]^2 \rangle} \approx -2\Delta. \tag{22}$$

It is known that this quantity gives almost exact roughness exponents for $r \ll \xi$ [52]. In Eq. (22), an average over different reference positions $\mathbf{r_0}$, different orientations, and independent samples are considered.

Following the same principle as described before and using Eq. (16), we obtain:

$$G(r,t) \approx K_G^I r^{2\alpha} + K_G^{II} + K_G^{III}\left(\frac{a}{r}\right)^2, \quad (23)$$

where $K_G^I = 2Ac_1$, $K_G^{II} = -2Ac_2 a^{2\alpha}$, and $K_M^{III} = -2Ac_3 a^{2\alpha}$. Similarly, the ratios for the measure G, as defined below, can be obtained:

$$R_{I,II,G} \equiv \frac{K_G^I}{K_G^{II}} = -\frac{c_1}{c_2}a^{-2\alpha}; \quad (24)$$

$$R_{I,III,G} \equiv \frac{K_G^I}{K_G^{III}} = -\frac{c_1}{c_3}a^{-2\alpha}; \quad (25)$$

and

$$R_{II,III,G} \equiv \frac{K_G^{II}}{K_G^{III}} = \frac{c_2}{c_3}. \quad (26)$$

From Eqs. (19)–(21) and Eqs. (24)–(26), we obtain (for $d = 1$ and the corresponding roughness exponent for the EW class, $\alpha = 0.5$):

$$\frac{R_{I,II,M}}{R_{I,II,G}} = \frac{2}{3}; \quad (27)$$

$$\frac{R_{I,III,M}}{R_{I,III,G}} = \frac{8}{15}; \quad (28)$$

and

$$\frac{R_{II,III,M}}{R_{II,III,G}} = \frac{4}{5}. \quad (29)$$

These results show that the TPS method is as accurate as deriving the exponents from G, at least for $d = 1$. We emphasise that the TPS method has a comparatively large length interval for such scaling for KPZ models (see Supplemental Material [53] for results of G measurements for KPZ models in $d = 1, 2$).

B. Villain-Lai-Das Sarma (VLDS) class

Next, we extend our analysis to the VLDS class. When diffusion is the dominant mechanism during the film growth, the space-time evolution of $h(\mathbf{x}, t)$, if the incoming particle flux is omitted, is described by the VLDS equation [also called nonlinear molecular-beam-epitaxy (nMBE) equation] [3,55,56]:

$$\frac{\partial h(\mathbf{x},t)}{\partial t} = -\nu_4 \nabla^4 h(\mathbf{x},t) + \lambda_4 \nabla^2 [\nabla h(\mathbf{x},t)]^2 + \eta(\mathbf{x},t), \quad (30)$$

where ν_4 and λ_4 are constants and $\eta(\mathbf{x}, t)$ is a nonconservative Gaussian noise described by Eq. (4). The scaling exponents β, α, and z for the VLDS equation were obtained by dynamic renormalization group analysis (RG) as follows:

$$\alpha = \frac{4-d}{3} - \varphi(d), \quad (31)$$

$z = (d + 8)/3 - 2\varphi(d)$ and $\beta = \alpha/z$. Here,

$$\varphi(d) = \begin{cases} 0 & \text{for one loop[56]}, \\ 0.01361(2 - d/2)^2 & \text{for two loops[57].} \end{cases} \quad (32)$$

Note that there is no proof that one of them are exact, i.e., both solutions are within the perturbative approach of RG. Local roughness exponents consistent with that ones where numerically achieved for $d = 1, 2$ [58,59].

We have performed our analysis here for $d = 2$, which are particularly relevant for applications, considering the conservative restricted solid-on-solid (CRSOS) model [60,61]. This model is connected with the nMBE universality class, since the surface dynamic is ruled by adatom diffusion. Our results are presented here for $L = 512$ (no significant differences were found for $L = 256$) and considering an average over 200 different samples. In the CRSOS model, one site is randomly selected for one adatom deposition. The height differences δh between nearest neighbors obey the restriction $\delta h \leqslant \delta H_{\max}$. In this work, we present the results for the case $\delta H_{\max} = 1$. If this condition is satisfied for the randomly chosen incidence site, the particle remains permanently stuck there. Otherwise, it searches for the nearest position where the condition is satisfied, which then becomes the location of deposition. In the case of multiple options, one of them is randomly chosen.

Figure 7 shows a comparison of the results for the height difference correlation function $G(r, t)$, the Higuchi method, and the method TPS. Importantly, only the TPS method was able to achieve an effective fractal dimension that (almost) matches that of the VLDS. However, this was not verified in a thin film regime. This result was limited to steady state (results for $t = 2^{26}$) and to a narrow range of scale lengths compared to the results for the KPZ class. Our results show that neither plateaus nor values consistent with those for VLDS were found for $G(r, t)$ and $\mathcal{L}_k$.

These results show that the determination of the fractal dimension for diffusion-dominated growth of thin films is still very problematic, possibly because the VLDS interfaces exhibit transient mounded behavior [58,59].

VI. CONCLUSION

Summarizing, in this work we analyzed the conditions for which the true fractal dimension could be extracted in the context of KPZ lattice models for $d = 1, 2$, which represent film growth. Our results revealed that, using the TPS method, the measure M, as defined in Eq. (7), scaled as $M = t^\delta g[\Theta]$, where $\delta = 2\beta$, $\Theta \equiv \tau t^{-1/z}$, and β and z are the growth and dynamic KPZ exponents. We showed that, in the steady state, which is not accessible experimentally, the effective fractal dimensions were consistent with those for KPZ for $d = 1, 2$, with all scale lengths up to the lateral size of the system. While this consistency has been observed by using the TPS method, the Higuchi method proved to be of more limited use, even in the steady state.

Importantly, in the growth of thin films, the true fractal dimensions obtained by the TPS method can be observed within a narrow range of spatial scale lengths, with the upper limit being of the same order of magnitude as the correlation length of the interface. If a thin film is considered for the measurement of a fractal dimension, a high resolution of the surface topography, such as that obtained from probe microscopy, is required to determine the surface fluctuations for small-scale lengths.
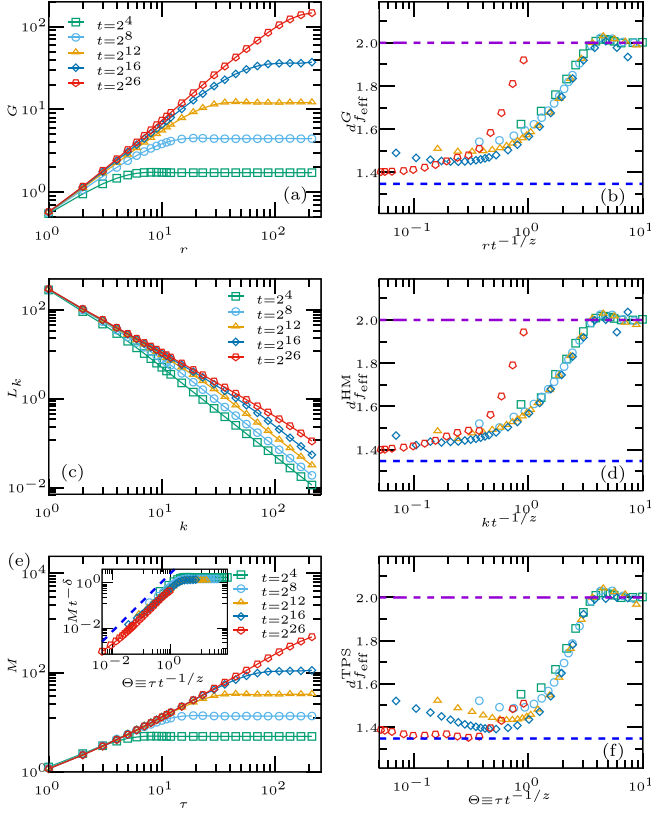
FIG. 7. Results for $d = 2$ and $L = 512$, considering the CRSOS model and an average over 200 different samples. (a) and (b) correspond to the results for the height difference correlation function, $G(r, t)$, and the effective fractal dimension $d_{f_{\text{eff}}}^{\text{G}}$, respectively. (c) and (d) correspond to the results for the measure $\mathcal{L}_k$ (Higuchi method), and the effective fractal dimension, $d_{f_{\text{eff}}}^{\text{HM}}$, respectively. (e) and (f) correspond to the results for the measure M (TPS method), and the effective fractal dimension, $d_{f_{\text{eff}}}^{\text{TPS}}$, respectively. The inset of (e) shows the collapse obtained by replacing the variables $M \rightarrow Mt^{-\delta}$ and $\tau \rightarrow \tau t^{-1/z}$, where z is the dynamic exponent and $\delta = 2\beta$ for the VLDS class (for a two-loop RG approximation). The slope shown in the inset has slope 2α, where α is given by Eqs. (31) and (32), considering a two loop RG approximation (see the text). In (b), (d), and (f), dashed horizontal bottom and top lines represent the values of the VLDS fractal dimension for $d = 2$, using Eq. (5) [$d_f = 2 - \alpha$], and the value 2, respectively.

When using the TPS method in this limit, our results showed that the true KPZ fractal dimensions were formally achieved if the condition $\tau t^{-1/z} \lesssim 0.3$ was satisfied. This range encompasses a very clear plateau region that include a thin film regime for the extraction of the fractal dimension. Such a feature has not been verified from the local roughness measurements, which have the same scaling properties of $\sqrt{G}$, using lattice models in order to extract the roughness

exponents (e.g., Ref. [62]). Indeed, the effective roughness exponents found in Ref. [62] showed inflection points at the corresponding universality class exponents, which will ultimately turn into plateaus with α equal to the asymptotic one. However, the deposition times will have to increase many orders of magnitude and, consequently, the deposit will not have the features of a thin structure anymore [62].

For a discussion of the limits of the inequality $\tau t^{-1/z} \lesssim 0.3$, let us consider the situation for $d = 2$. If we consider times $10 \leqslant t \leqslant 10^4$, the corresponding upper limits for the scale lengths are in the range $1 \lesssim \tau_{\text{max}} \lesssim 10^2$. Indeed, the lattice parameter of a crystal is usually on the order of a few Å units. Thus, if we assume $a \approx 0.3$ nm, then for a film made up to $t = 10^4$ we would have $\tau_{\text{max}} \approx 30$ nm. This example illustrates the difficulty of achieving a wide range of scale lengths to measure an effective fractal dimension using the methods studied in this work. Using the TPS method for an experimental KPZ growth would certainly be interesting to investigate the above limitations. For some recent atomic force microscopy (AFM) experiments showing KPZ growth, see Refs. [30,32,63,64].

Scaling corrections for the measure M and the height difference correlation function were analytically examined and compared for the class EW in $d = 1$, yielding similar accuracy for both methods. Importantly, we extend our discussion to a model representing diffusion-dominated growth of thin films for $d = 2$. We have found that the method TPS is the only method studied here that can theoretically achieve an effective fractal dimension consistent with that of the VLDS class. However, this was found at steady state and within a narrow range of the length scale, compared to the results for the KPZ class. These results suggest that determining the fractal dimension for diffusion-dominated growth of thin films is problematic, at least theoretically and with the methods discussed here. Therefore, the investigation and development of new methods to achieve an effective fractal dimension consistent with that of the VLDS class in a thin film regime is certainly desirable.

[1] J. Krug, Adv. Phys. **46**, 139 (1997).

[2] M. Ohring, *Materials Science of Thin Films: Depositon & Structure* (Elsevier Science, Amsterdam, 2002).

[3] A. L. Barabási and H. E. Stanley, *Fractal Concepts in Surface Growth* (Cambridge University Press, Cambridge, 1995).

[4] S. F. Edwards and D. R. Wilkinson, Proc. Roy. Soc. Lond. A **381**, 17 (1982).

[5] M. Kardar, G. Parisi, and Y.-C. Zhang, Phys. Rev. Lett. **56**, 889 (1986).

[6] J. Krug, P. Meakin, and T. Halpin-Healy, Phys. Rev. A **45**, 638 (1992).

[7] B. Derrida, Phys. Rep. **301**, 65 (1998).

[8] A. Hansen, J. Schmittbuhl, G. G. Batrouni, and F. A. de Oliveira, Geophys. Res. Lett. **27**, 3639 (2000).

[9] B. A. Mello, A. S. Chaves, and F. A. Oliveira, Phys. Rev. E **63**, 041113 (2001).

[10] C. Castelnovo, A. Podestà, P. Piseri, and P. Milani, Phys. Rev. E **65**, 021601 (2002).

[11] M. S. Gomes-Filho, A. L. Penna, and F. A. Oliveira, Results Phys. **26**, 104435 (2021).

[12] P. H. R. dos Anjos, M. S. Gomes-Filho, W. S. Alves, D. L. Azevedo, and F. A. Oliveira, Front. Phys. **9**, 741590 (2021).

[13] E. E. M. Luis, T. A. de Assis, and F. A. Oliveira, J. Stat. Mech.: Theory Exp. (2022) 083202.

[14] F. Family and T. Vicsek, J. Phys. A: Math. Gen. **18**, L75 (1985).

[15] F. D. A. Aarão Reis, Phys. Rev. E **88**, 022128 (2013).

[16] S. G. Alves, C. I. L. de Araujo, and S. C. Ferreira, New J. Phys. **18**, 093018 (2016).

[17] F. Lechenault, G. Pallares, M. George, C. Rountree, E. Bouchaud, and M. Ciccotti, Phys. Rev. Lett. **104**, 025502 (2010).

[18] Z. Zhang, S. Ispas, and W. Kob, Phys. Rev. Lett. **126**, 066101 (2021).

[19] Y. Romaguera-Barcelay, A. Pedraça, J. Moreira, A. Almeida, P. Tavares, W. Brito, R. Matos, M. Pires, E. Pinto, and H. da Fonseca Filho, Mater. Sci. Eng., B **267**, 115090 (2021).

[20] W. Zhu, E. Mohammadi, and Y. Diao, J. Polym. Sci., Part B: Polym. Phys. **57**, 1622 (2019).

[21] Kavyashree, R. Pandey, R. Yadav, M. Kumar, H. Bhasker, A. Mittal, A. Pandey, and S. Pandey, Appl. Surf. Sci. **466**, 780 (2019).

[22] S. Tălu, R. P. Yadav, A. K. Mittal, A. Achour, C. Luna, M. Mardani, S. Solaymani, A. Arman, F. Hafezi, A. Ahmadpourian, S. Naderi, K. Saghi, A. Méndez, and G. Trejo, Opt. Quantum Electron. **49**, 256 (2017).

[23] K. Ghosh and R. K. Pandey, AIP Conf. Proc. **2115**, 030280 (2019).

[24] W. Zhou, Y. Cao, H. Zhao, Z. Li, P. Feng, and F. Feng, Fractal Fract. **6**, 135 (2022).

[25] J. Kondev, C. L. Henley, and D. G. Salinas, Phys. Rev. E **61**, 104 (2000).

[26] J. M. Kim and J. M. Kosterlitz, Phys. Rev. Lett. **62**, 2289 (1989).

[27] P. Meakin, P. Ramanlal, L. M. Sander, and R. C. Ball, Phys. Rev. A **34**, 5091 (1986).

[28] M. Plischke, Z. Rácz, and D. Liu, Phys. Rev. B **35**, 3485 (1987).

[29] D. Liu and M. Plischke, Phys. Rev. B **38**, 4781 (1988).

[30] R. A. Almeida, S. O. Ferreira, I. Ferraz, and T. J. Oliveira, Sci. Rep. **7**, 1 (2017).

[31] F. D. A. Aarão Reis, Phys. Rev. E **72**, 032601 (2005).

[32] R. A. L. Almeida, S. O. Ferreira, T. J. Oliveira, and F. D. A. Aarao Reis, Phys. Rev. B **89**, 045309 (2014).

[33] E. A. Rodrigues, F. A. Oliveira, and B. A. Mello, Acta Phys. Pol. B **46**, 1231 (2015).

[34] W. S. Alves, E. A. Rodrigues, H. A. Fernandes, B. A. Mello, F. A. Oliveira, and I. V. L. Costa, Phys. Rev. E **94**, 042119 (2016).

[35] I. S. S. Carrasco and T. J. Oliveira, Phys. Rev. E **98**, 010102(R) (2018).

[36] W. P. Gomes, A. L. A. Penna, and F. A. Oliveira, Phys. Rev. E **100**, 020101(R) (2019).

[37] E. Daryaei, Phys. Rev. E **101**, 062108 (2020).

[38] Y. Zhou, Y. Li, H. Zhu, X. Zuo, and J. Yang, Fractals **23**, 1550016 (2015).

[39] W. H. Press, S. A. Teukolsky, W. T. Vetterling, and B. P. Flannery, *Numerical Recipes 3rd Edition: The Art of Scientific Computing*, 3rd ed. (Cambridge University Press, New York, 2007).

[40] G. Ódor, B. Liedke, and K.-H. Heinig, Phys. Rev. E **79**, 021125 (2009).

[41] T. J. Oliveira, S. G. Alves, and S. C. Ferreira, Phys. Rev. E **87**, 040102(R) (2013).

[42] J. Kelling, G. Ódor, and S. Gemming, Phys. Rev. E **94**, 022107 (2016).

[43] T. J. Oliveira, Phys. Rev. E **106**, L062103 (2022).

[44] D. Siniscalco, M. Edely, J.-F. Bardeau, and N. Delorme, Langmuir **29**, 717 (2013).

[45] F. D. A. A. Reis, J. Stat. Mech.: Theory Exp. (2015) P11020.

[46] T. A. de Assis and F. D. A. Aarão Reis, Phys. Rev. E **92**, 052405 (2015).

[47] A. Pagnani and G. Parisi, Phys. Rev. E **92**, 010101(R) (2015).

[48] T. Higuchi, Physica D **31**, 277 (1988).

[49] H. Ahammer, N. Sabathiel, and M. A. Reiss, Chaos **25**, 073104 (2015).

[50] T. Antal, M. Droz, G. Györgyi, and Z. Rácz, Phys. Rev. Lett. **87**, 240601 (2001).

[51] T. Antal, M. Droz, G. Györgyi, and Z. Rácz, Phys. Rev. E **65**, 046140 (2002).

[52] D. O. Mallio and F. Aarão Reis, Physica A **596**, 127178 (2022).

[53] See Supplemental Material at http://link.aps.org/supplemental/10.1103/PhysRevE.107.034802 for results of G measurements for KPZ models in $d = 1, 2$.

[54] Y. Zhao, G.-C. Wang, and T.-M. Lu, *Characterization of Amorphous and Crystalline Rough Surface: Principles and Applications*, Series: Experimental Methods in the Physical Sciences (Elsevier, Amsterdam, 2001), Vol. 37, pp. xv-xvii.

[55] J. Villain, J. Phys. I (France) **1**, 19 (1991).

[56] Z.-W. Lai and S. Das Sarma, Phys. Rev. Lett. **66**, 2348 (1991).

[57] H. K. Janssen, Phys. Rev. Lett. **78**, 1082 (1997).

[58] E. E. M. Luis, T. A. de Assis, and S. C. Ferreira, Phys. Rev. E **95**, 042801 (2017).

[59] E. E. M. Luis, T. A. de Assis, S. C. Ferreira, and R. F. S. Andrade, Phys. Rev. E **99**, 022801 (2019).

[60] Y. Kim, D. K. Park, and J. M. Kim, J. Phys. A: Math. Gen. **27**, L533 (1994).

[61] Y. Kim and J.-M. Kim, Phys. Rev. E **55**, 3977 (1997).

[62] A. Chame and F. Aarão Reis, Surf. Sci. **553**, 145 (2004).

[63] T. Halpin-Healy and G. Palasantzas, Europhys. Lett. **105**, 50001 (2014).

[64] R. A. L. Almeida, S. O. Ferreira, I. R. B. Ribeiro, and T. J. Oliveira, Europhys. Lett. **109**, 46003 (2015).